PubMed Central Search Journal List

NIH Public Access
Author Manuscript
Accepted for publication in a peer reviewed journal

About Author manuscripts | Submit a manuscript

Journal List > NIHPA Author Manuscripts

Circ Cardiovasc Imaging. Author manuscript; available in PMC 2010 October 15.
Published in final edited form as:
Circ Cardiovasc Imaging. 2010 July 1; 3(4): 464–472.
Published online 2010 May 4. doi: 10.1161/CIRCIMAGING.109.896654.

PMCID: PMC2955298
NIHMSID: NIHMS243796

Copyright notice and Disclaimer

Molecular Imaging of Atherosclerotic Plaques Targeted to Oxidized LDL Receptor LOX-1 Using SPECT/CT and Magnetic Resonance

Dayuan Li, MD, PhD,[*] Amit Patel, MD,[¥] Alexander L. Klibanov, PhD,[*] Christopher M. Kramer, MD,[Δ*] Mirta Ruiz, MD,[*] Bum-Yong Kang, PhD,[#] Jawahar L. Mehta, MD, PhD,[#] George A. Beller, MD,[*] David K. Glover, PhD,[*®] and Craig H Meyer, PhD[†®]

[*]Cardiovascular Division, University of Virginia, Charlottesville, VA 22908
[¥]Section of Cardiology, University of Chicago, Chicago, IL 60637
[Δ]Department of Radiology, University of Virginia, Charlottesville, VA 22908
[#]Division of Cardiovascular Medicine, University of Arkansas for Medical Sciences, Little Rock, AR 72205
[†]Department of Biomedical Engineering, University of Virginia, Charlottesville, VA 22908
Address for correspondence: David K Glover® (Email: dglover@virginia.edu) and Craig H Meyer®, (Email: cmeyer@virginia.edu) contributed equally to this work. University of Virginia Health System, PO Box 800500, Charlottesville, VA 22908. Phone: (434) 243-2784 Fax: (434) 924-5585

The publisher's final edited version of this article is available at Circ Cardiovasc Imaging

Background

The oxidized-LDL receptor LOX-1 plays a crucial role in atherosclerosis. We sought to detect and assess atherosclerotic plaque *in vivo* using SPECT/CT and magnetic resonance imaging (MRI) using a molecular probe targeted at LOX-1.

Methods & Results

Apo $E^{-/-}$ mice on Western diet and $LDLR^{-/-}$ and $LDLR^{-/-}$/$LOX\text{-}1^{-/-}$ mice on atherogenic diet were used. Imaging probes consisted of liposomes decorated with LOX-1 antibodies (LOX-1) or nonspecific IgG (nIgG), ^{111}In or gadolinium (Gd), and DiI fluorescence markers. *In vivo* imaging was performed 24 hrs after intravenous injection (150 μl) of LOX-1 (or nIgG) probes labeled with either ^{111}In (600 μCi) or Gd (0.075 mmol/kg) followed by aortic excision for phosphor imaging and Sudan IV staining or fluorescence imaging and H&E staining. The LOX-1 probe was also co-localized with specific cell types, apoptosis, and MMP9 expression using frozen aortic sections.

SPECT/CT imaging of the LOX-1 probe showed aortic arch hotspots in Apo $E^{-/-}$ mice (n=8), confirmed by phosphor imaging. MRI showed significant Gd enhancement in atherosclerotic plaques in $LDLR^{-/-}$ mice with the LOX-1 (n=7), but not nIgG, probe (n=5). No signal enhancement was observed in $LDLR^{-/-}$/$LOX\text{-}1^{-/-}$ mice injected with LOX-1 probe (n=5). These results were confirmed by *ex-vivo* fluorescence imaging. The LOX-1 probe bound preferentially to the plaque shoulder, a region with vulnerable plaque features including extensive LOX-1 expression, macrophage accumulation, apoptosis and MMP9 expression.

Conclusions

LOX-1 can be used as a target for molecular imaging of atherosclerotic plaque *in vivo*. Furthermore, LOX-1 imaging may identify rupture-prone atherosclerotic plaque.

Keywords: Molecular imaging, LOX-1, atherosclerotic plaque, SPECT, MRI

Atherosclerosis is a major cause of many cardiovascular disease states including myocardial ischemia, acute myocardial infarction and stroke. There are currently no established non-invasive methods for identifying the rupture-prone atherosclerotic plaque in the living animal. Molecular tools are rapidly being developed to elucidate molecular and cellular processes leading to apoptosis, collagen synthesis and degradation, inflammation, angiogenesis and changes in the structural components of the plaque.

Many studies have demonstrated that oxidized low density lipoprotein (ox-LDL) plays a critical role in atherogenesis (1–3). The ox-LDL receptor LOX-1 mediates the pathological effects of ox-LDL in atherosclerotic lesions (2,3). LOX-1 is a type II transmembrane protein with a short intracellular cytoplasmic tail and a long extracellular domain containing a C-type lectin-like structure (3). LOX-1 induces free radical generation (4), apoptosis of endothelial cells and monocytes/macrophages (5,6), expression of adhesion molecules (7) and activates the inflammatory cascade (8,9). LOX-1 also induces expression and activation of matrix metalloproteinases (MMPs) (10). These pathological effects of LOX-1 not only initiate atherosclerotic lesion formation, but also contribute to the vulnerability of a plaque to rupture. A recent study (11) demonstrated that LOX-1 deficiency significantly decreases the formation of atherosclerotic lesions.

We have developed a novel non-invasive imaging probe targeted to LOX-1. We tested the binding of this LOX-1 probe to atherosclerotic lesions *in vivo* and used this technique to detect and assess atherosclerotic plaque using SPECT/CT and MRI.

Imaging probe

Liposomes consisted of 1,2-Dioleoyl-sn-Glycero-3-Phosphocholine(Avanti Lipids, Alabaster, AL), cholesterol (Sigma), N-hydroxysuccinimide ester of carboxy-PEG3400-DSPE (Shearwater Polymers) and DiI (Invitrogen) at the mass ratio of 50:25:25:1. For MRI studies, diethylenetriaminepentaacetic acid α, ω-bis (8-stearoylamido-3,6-diaoxaoctylamide) gadolinium complex (Sigma) was added at 1:1 mass ratio with phosphatidylcholine. Lipids were dissolved in chloroform and subjected to rotary evaporation in a glass vial under vacuum to create a thin uniform layer of dry lipid on the glass surface. Citrate buffer (10mM, pH 4.4) was quickly added, mixture agitated to prepare multilamellar liposomes, and then rapidly passed through a 100 nm filter 40 times using a Liposofast device (Avestin). Liposomes (~100 nm in size) were immediately mixed with LOX-1 or nonspecific IgG antibody (R&D Systems, 250 μg in 10 mM HEPES buffer, pH 8.0) overnight at 4°C, so that covalent coupling between the protein aminogroup and activated carboxyl of PEG-lipid would occur. The compounds were subjected to ultracentrifugation at 45,000 rpm (50Ti rotor, Beckman Coulter ultracentrifuge) for 30 min to remove free antibodies. Finally, the immunoliposome pellets (probes) were dispersed in PBS buffer. For ^{111}In labeling, liposomes carried a trace amount of DTPA-phosphatidylethanolamine. The liposome preparations were mixed with ^{111}In (Perkin Elmer Life Sciences) in acetate buffer (0.5 M, pH 6.0) for 2 hrs at room temperature and then filtered by a single passage through a Sephadex G50 gel column under centrifugation at 1000 g for 1 min. The imaging probe consisted of liposomes decorated with anti-LOX-1 antibody (LOX-1 probe) or non-specific nIgG (nIgG probe), ^{111}Indium (SPECT) or Gadolinium (MRI), and DiI fluorescence markers.

Dot blot analysis

LOX-1 antigen (R&D system) (200 ng) was placed on a nitrocellulose membrane, dried, and blocked with 3% BSA for 1 hr. The membranes were

incubated with serial dilutions (0.06 to 4 nM LOX-1 antibody concentrations) of ^{111}In-liposome-LOX-1-Ab-DiI at room temp for 2 hrs, and then exposed to a phosphor imaging plate for 90 min, followed by gamma well counting of each dot.

Solid phase binding assay

LOX-1 antigen (200 ng in 0.1 ml PBS) was placed into each well of a standard 96-well ELISA plate overnight, washed with PBS, and then blocked with 3% BSA for 1 hr. Serial dilutions (0.1 to 14 nM LOX-1 antibody concentrations) of Gd-liposome-LOX-1-Ab-DiI were added to each well and incubated at room temp for 2 hrs. The plate was washed with PBS 4 times. Fluorescence intensity of antigen-bound liposomes was determined with a microplate reader (Gemini XS, Molecular Devices). A control probe experiment with Gd-liposome-nIgG-DiI was performed in parallel to evaluate nonspecific binding.

Animal protocol

The University of Virginia of Animal Care and Use Committee approved all animal experiments. ApoE $^{-/-}$ mice were placed on Western diet (Harlan) for over 20 weeks and used for SPECT/CT imaging. Mice were anesthetized with isoflurane and injected intravenously with 150 μL of LOX-1 or nIgG probe with ~600 μCi of ^{111}In. SPECT/CT imaging was performed 24 hrs after injection followed by aortic excision. Aortas (n=6) were either longitudinally opened and exposed to phosphor imaging plate for 90 min, followed by Sudan IV staining to identify atherosclerotic lesions, or they were fixed with 4% paraformaldehyde overnight and sent to the UVA Core Pathology Laboratory for analysis of frozen sectioning (n=6).

LDLR$^{-/-}$ (Jackson Laboratories) and LDLR$^{-/-}$/LOX-1$^{-/-}$ (10) mice were fed an atherogenic diet (Harlan) for 16 weeks. Mice were anesthetized with isoflurane and intravenously injected with 150 μL of LOX-1 (n=12) or nIgG probe (n=5) with 0.075 mmol Gd/kg. MR imaging (7.0T, Clinscan, Bruker/Siemens) was performed at baseline and again 24 hrs after injection. The aortas were then excised for frozen sectioning to examine binding of probe in the atherosclerotic plaques and for H&E and immunostaining.

Blood pool clearance and tissue biodistribution of probes

Wild-type C57BL/6 9 (n=6) and Apo E$^{-/-}$ mice (n=8) were anesthetized with isoflurane and intravenously injected with the LOX-1 or nIgG probe with ~600 μCi of ^{111}In. Five μl of blood was collected at 15 sec, 30 sec, 1 min, 15 min, 30 min, 1h, 2h, 4h and 24 hrs from the tail vein. Blood pool activity was decay-corrected and normalized by dividing by initial blood pool counts. Twenty four hours after injection, tissues from heart, lung, liver, fat, muscle, kidney, spleen and gut, and urine were collected. Decay-corrected tissue radioactivity was calculated by γ-counts per mg tissue wet weight per time unit and then divided by blood pool radioactivity at 24 hrs.

Confocal Microscopy

Frozen aortic sections were washed of dextrose with PBS buffer and blocked with 3% BSA for 1 hr, and then incubated with a FITC adsorbed rabbit anti-mouse macrophage antibody (1:50 dilution, Cedarlane Laboratories) and a Dylight 633 Red (Thermo Scientific) labeled goat anti-mouse antibody to smooth muscle cells (1:100 dilution, Santa Cruz) diluted in 3% BSA overnight at 4°C. The sections were then washed in PBS buffer 4 times for 5 min each and incubated with DAPI (1 μg/ml) for 10 min. The sections were washed again with PBS and mounted with anti-fade medium. Confocal imaging was performed within 24 hrs using a Zeiss LSM 510 META microscope in an inverted configuration. The detectors were configured for blue, green, red and far-red emission detection (filters: band pass 420–480 nm, 505–530 nm, 560–615 nm and 650 nm). Pinhole settings were adjusted for equal “optical sections”.

Fluorescent TUNEL staining

In situ nick end-labeling (TUNEL) and propidium iodide staining was performed as described previously (5,12). In brief, frozen sections on slides were incubated with 0.3 U/μl terminal deoxynucleotidyl transferase (TDT) and 0.04 nmol/μl fluorescein-12-dUTP (Promega) in TDT buffer for 60 min at 37°C. Unincorporated fluorescein-dUTP was removed, and the slides were immersed in 1 μg/ml of propidium iodide in PBS for 15 min. The negative controls were performed without TDT enzyme.

Fluorescent immunostaining

Details of immunostaining have been provided previously (11,12). In brief, 5 μm thick frozen sections from aortas were incubated with rabbit anti-mouse MMP9 antibody (sc-6840, Santa Cruz) overnight at 4°C. Sections were rinsed in PBS buffer 4 times, and incubated with secondary antibody goat anti-rabbit IgG-FITC (Santa Cruz). Sections were rinsed with PBS buffer 4 times and then mounted with anti-fade medium. The negative controls were prepared using secondary antibody alone.

SPECT/CT imaging protocol

SPECT/CT imaging was performed using a dual-head camera with 1 mm pinhole apertures. A complete SPECT data set consisted of 60 projections at 6 degree increments at 30 sec per projection. The images were reconstructed using a maximum-likelihood expectation maximization (MLEM) algorithm. CT was performed before (without contrast) and after (with contrast) SPECT imaging. A complete CT data set consisted of 216 projection images acquired at one degree increments over 5 minutes. The intravascular agent Fenestra® (Cat# LC-131, ART Inc.) was used to provide CT contrast.

MRI scan protocol

MRI of the ascending aorta was performed with a T1-weighted black-blood spiral gradient-echo sequence (echo time 1.2 ms; flip angle 90°; field of view 3×3 cm; 135 interleaves; readout window 4.1 ms; spatial resolution 67 μm) with 11 contiguous 0.5 mm-thick slices. Cardiac-gated double-inversion pulses for suppression of the blood signal were interleaved with cardiac-gated spiral readouts, resulting in an effective repetition time for the readouts of two R-R intervals. Four signal averages with cardiac and respiratory gating were used, for a total imaging time of 2.5 minutes per slice. For the post-injection scan, the slices were matched to the baseline pre-injection scan using the origin of the left main and LAD coronary artery as anatomic landmarks. To quantify the MRI results, signal intensity (SI) was measured in 4 aortic wall regions of interest as well as the aortic lumen and muscle on each slice at both time points. The standard deviation of noise was also recorded for each slice. These measurements were recorded for all slices at every time point imaged. The contrast-to-noise ratio (CNR) of aortic wall to lumen was calculated for each slice. %CNR = (CNR post – CNR pre-injection)/CNR pre-injection. The normalized enhancement ratio (NER) was defined as the average post-contrast SI from 4 regions of interest within the aortic wall divided by the muscle SI in the same slice and then divided by the pre-contrast SI. %NER = (NER-1) × 100. In this study, %CNR and %NER were used to present the summarized MRI data (13).

Data Analysis

Data represent mean of at least three independently performed experiments. Data are presented as mean ± SD. Data were analyzed by ANOVA, followed by a Bonferroni correction. A *P* value of less than 0.05 was considered to be statistically significant.

Binding analysis of probes in vitro

As shown in Figure 1, anti-LOX-1 antibody-linked liposomes successfully bound to LOX-1 antigen-coated surfaces. This was demonstrated by Dot blot analysis using the LOX-1 probe (^{111}In-liposome-LOX-1 antibody-DiI) (left panel). Fluorescence-labeled solid phase binding assay also showed that the LOX-1 probe (Gd-liposome-LOX-1 antibody-DiI) bound to LOX-1 antigen in a sigmoid curve pattern, whereas, the nIgG probe (Gd-liposome-nIgG-DiI) showed very little binding to LOX-1 antigen (right panel).

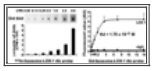

Figure 1

LOX-1 probe (^{111}In-liposome-LOX-1 Antibody-DiI) binding to LOX-1 antigen *in vitro*. Left top panel is a representative dot blot analysis. The mean data from 3 separate experiments are shown in the left lower panel. Right panel shows that LOX-1 probe (Gd-liposome-LOX-1 antibody-DiI) bound to LOX-1 antigen *in vitro* by ELISA. The non-specific IgG (nIgG) probe (Gd-liposome-nIgG-DiI) showed no binding to LOX-1 antigen (n=3).

Blood pool clearance and tissue bio-distribution in vivo

LOX-1 and nIgG probes had similar blood clearance rate in wild type C57BL/6 mice (Fig 2, left upper panel). However, LOX-1 probes cleared more slowly than nIgG probes initially after injection ($P<0.05$ at different time points) in the ApoE$^{-/-}$ mice. There was no significant difference in clearance of the two probes at 24 hours post-injection (Fig 2, right upper panel). Based on the blood pool clearance data, SPECT/CT and MR imaging was performed at 24 hrs post injection of the probe.

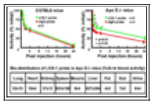

Figure 2

Blood pool clearance of probes in C57BL6 and Apo E$^{-/-}$ mice (top panel). Blood pool clearance of LOX-1 and nIgG probes was similar in wild type C57BL6 mice (left upper panel). LOX-1 probes cleared slowly compared to nIgG probes in the Apo E$^{-/-}$ mice. However, there was no difference in clearance between the two probes at 24 hrs (right upper panel). Bottom panel shows tissue bio-distribution. LOX-1 probes accumulated mainly in liver and spleen.

As expected, both probes largely accumulated in the liver and spleen because of their liposome nature and the presence of Fc fragments on the antibody or IgG molecules on the liposome surface.

LOX-1 expression, LOX-1 probe binding in plaque in vivo

By immunostaining, we showed that LOX-1 was highly expressed in atherosclerotic plaques, especially in the shoulder area (Figure 3, left panel). Consistent with this finding, most of the LOX-1 probe binding was also observed in this same region (Figure 3, middle panel). Notably, we found that LOX-1 probe did not bind to every atherosclerotic plaque *in vivo*. In contrast to the extensive binding of the LOX-1 probe, there was negligible nIgG probe binding to the atherosclerotic plaque *in vivo* (Figure 3, right panel).

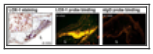

Figure 3

LOX-1 expression and LOX-1 probe binding in atherosclerotic plaque. LOX-1 is highly expressed in atherosclerotic plaques, especially in the shoulder region (left panel). The LOX-1 probe bound mainly to the shoulder area of the atherosclerotic plaque (middle panel). There was little binding of the nIgG probe (right panel). L – lumen.

Co-localization of LOX-1 probe binding to cells within atherosclerotic plaque in vivo

To further characterize specific cell lines within the plaque to which LOX-1 probe

binds, we performed fluorescent immunostaining for macrophages and smooth muscle cells in frozen aortic sections taken from Apo $E^{-/-}$ mice injected with LOX-1 probes. Confocal microscopy showed that a vast amount of LOX-1 probe co-localized with macrophages in the atherosclerotic plaque, with little co-localization with proliferated smooth muscle cells (Figure 4).

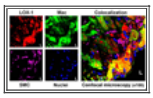

Figure

Confocal microscopic images of aortic sections. LOX-1 probe in plaque appears red; macrophages appear green; smooth muscle cells appear purple and nuclei are blue. LOX-1 probe is co-localized mainly with macrophages in the atherosclerotic plaque (yellow = overlap of red and green). There was little LOX-1 probe co-localization with proliferating smooth muscle cells.

LOX-1 probe binding, apoptosis and matrix metalloproteinase

Next, we examined the relationship between the *in vivo* LOX-1 imaging signal and other typical markers of a vulnerable plaque including apoptosis and MMP9 expression. As shown in Figure 5, LOX-1 probe binding was co-localized with apoptotic cells (Figure 5, left panel) as well as MMP9 (right panel). Notably, there were few apoptotic cells or little MMP9 expression in regions of the plaque with minimal or no LOX-1 probe binding.

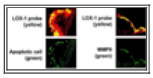

Figure

LOX-1, apoptosis and MMP9 expression in the plaque. LOX-1 probe binding (yellow color) was co-localized with apoptotic cells (green, left panel) and with cells expressing MMP9 (green, right panel).

SPECT/CT imaging, phosphor imaging and Sudan I staining

As shown in Figure 6, there were no hotspots detected by *in vivo* SPECT or *ex vivo* phosphor imaging in Apo $E^{-/-}$ mice injected with nIgG probe (top row). In contrast, all mice injected with LOX-1 probe had hotspots in the atherosclerotic region of the aortic arch by *in vivo* SPECT and *ex vivo* phosphor imaging (bottom row). There were no differences in the extent of atherosclerotic lesions between two groups determined by Sudan IV staining.

Figure

SPECT(A) and *ex vivo* phosphor imaging (C) showed no focal aortic arch hotspots in Apo $E^{-/-}$ mice injected with nIgG probe, whereas all Apo $E^{-/-}$ mice injected with LOX-1 probe had hotspots in the aortic arch (B- sagittal, coronal and transverse planes), confirmed by *ex vivo* phosphor imaging (D). Sudan IV staining demonstrated comparable plaques between the two groups (E&F).

MR imaging, fluorescence imaging and &E staining

Strong post-injection gadolinium enhancement was visualized in the aortic root and the arch in $LDLR^{-/-}$ mice injected with LOX-1 probe (Fig 7, left panel). These findings were confirmed by *ex vivo* fluorescence imaging of frozen sections that showed LOX-1 probe binding in the same area. The size of atherosclerotic plaque was confirmed by H&E staining. Post-Gd enhancement was not seen in the $LDLR^{-/-}$ mice injected with nIgG probe (Fig 7, middle panel). Furthermore, the specificity of LOX-1 probe binding was confirmed using $LDLR^{-/-}$/ $LOX\text{-}1^{-/-}$ double knockout mice that showed no post-Gd enhancement and no LOX-1 probe binding to plaque (Fig 7, right panel). These mice also showed fewer atherosclerotic lesions on H&E staining in agreement with previous studies (10). Quantitative MRI data (right panel) showed that $LDLR^{-/-}$ mice injected with LOX-1 probe had significantly higher contrast to noise ratio (CNR) and normalized enhancement ratio (NER) than the other two control groups, $LDLR^{-/-}$ mice injected with nIgG probe and $LDLR^{-/-}$/$LOX\text{-}1^{-/-}$ mice injected with LOX-1 probe.

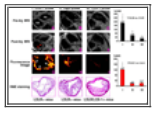

Figure

MRI showed post-injection gadolinium enhancement in aortic root to arch in the LDLR$^{-/-}$ mice injected with LOX-1 (D), but not nIgG probes (E), compared to pre-injection imaging (A & B). Fluorescence imaging of frozen sections confirmed LOX-1 probe binding (yellow color) in the same plaque area (G) with little nonspecific nIgG probe binding (H). Post-gadolinium enhancement was not seen in LDLR $^{-/-}$/LOX-1$^{-/-}$ double knockout mice injected with LOX-1 probes (F vs C), nor was LOX-1 probe binding seen in plaque from these mice (I). H&E staining (bottom row) shows the size of atherosclerotic plaque from adjacent fluorescent imaging sections. Quantitative MRI data (right panel) showed that LDLR$^{-/-}$ mice injected with LOX-1 probe increased contrast to noise ratio (CNR) and normalized enhancement ratio (NER) compared with the two control groups. PA-pulmonary artery. AA- ascending aorta.

Specific non-invasive techniques are needed to detect atherosclerotic plaque vulnerability and to monitor changes in these parameters. Development of such approaches requires delineation of appropriate markers of atherosclerosis and use of non-invasive imaging tags directed at these markers. To date, most invasive (intravascular ultrasound) and noninvasive (CT angiography) techniques for plaque imaging identify only the presence and extent of atherosclerotic plaque and do not image specific targets related to vulnerability.

Several studies have suggested that activation of the ox-LDL receptor LOX-1 induces endothelial dysfunction, enhances ox-LDL uptake in monocytes/macrophages and induces a state of oxidative stress. Accordingly, it has been suggested that LOX-1 is involved in the initiation and progression of atherosclerotic plaque (3,5,7–11,13). Indeed, recent studies show that deletion of LOX-1 reduces the progression of atherosclerosis (11). Furthermore, LOX-1 activates MMPs (10) resulting in collagen degradation and initiation of plaque rupture- the most proximate cause of acute coronary syndromes. Circulating levels of soluble LOX-1 are increased in patients with unstable coronary syndromes (14).

We validated molecular imaging of LOX-1 protein to detect atherosclerotic plaque using SPECT/CT and MR imaging techniques in two different models of atherosclerosis, the Apo E$^{-/-}$ and LDLR$^{-/-}$ mice on a high cholesterol diet. We found that the LOX-1 probe given intravenously specifically bound to atherosclerotic plaques, especially in the cap and shoulder areas, and could be clearly detected by both SPECT/CT and MR imaging of the aortic arch. Importantly, we found that the LOX-1 signal in the atherosclerotic plaque co-localized with macrophages, apoptotic cells and MMP9 expression. It is well known that plaques that are prone to rupture contain large numbers of inflammatory and apoptotic cells, and these regions secrete large amount of MMP9.

Molecular imaging probes for detecting atherosclerotic plaque

The ideal probe should target proteins expressed in the atherosclerotic plaque specifically and extensively, and it should have a high binding affinity and a high sensitivity and selectivity to target/s in the atherosclerotic plaque. Based on these criteria, various investigators have targeted different proteins and components of plaque to image atherosclerotic plaque *in vivo*. Apoptosis resulting in a loss of cell density in the plaque is an important component of atherosclerosis (15–17), although its precise significance and the timing of its appearance in the atherosclerotic region remains a subject of conjecture. Sarai et al (18) used radiolabeled annexin-V to detect apoptosis in the atherosclerotic plaque in a rabbit model. It is now well recognized that atherosclerotic lesions

contain a large number of monocytes/macrophages as part of the inflammatory process, and the number of inflammatory cells predict vulnerability of plaque to rupture (17,19,20). Accordingly, some studies targeted macrophages using Gd-immunomicelles for MRI in Apo $E^{-/-}$ mice (13) and iodinated nanoparticles dispersed with surfactant for CT imaging in rabbits (21). As mentioned earlier, enhanced MMP expression and activity causes degradation of collagen in cap and thus the tendency of plaque rupture (20,22). Accordingly, some studies (23,24) have targeted MMPs to detect atherosclerotic plaque in Apo $E^{-/-}$ and $LDLR^{-/-}$ mice and rabbits. Other studies have targeted ox-LDL (25), VCAM-1 (26), fibrin-binding peptide derivatives (27), and $\alpha_v\beta_3$ (28,29). These imaging targets, however, represent only a few components of atherosclerotic plaque.

The rationale for targeting LOX-1 in this study was that this molecule is highly expressed in advanced atherosclerotic plaque (11,12) in activated endothelial cells, macrophages, platelets and dendritic cells (12,30,31). Besides being highly expressed, its activation leads to apoptosis (5), free radical generation (4), inflammatory cell recruitment (7–9), and expression of MMPs (10) and tissue factor (32). Therefore, LOX-1 as a molecular imaging target may represent the full spectrum of pathological processes in atherosclerotic plaque. A recent study used ^{99m}Tc-LOX-1 antibody to detect atherosclerotic plaque in a rabbit model (33). However, use of this imaging probe was limited by low spatial resolution and poor signal to noise ratio because the half life of ^{99m}Tc is about 6 hours and an antibody usually takes longer than 6 hours to bind to an antigen *in vivo*.

In the current study, we constructed imaging probes using liposome vectors to carry the LOX-1 antibody, fluorescent marker DiI, and ^{111}In or Gd. The size of the liposome was kept less than 100 nm so that the liposomes could leave the vasculature, enter interstitial space and bind to the appropriate components of the atherosclerotic plaque. The liposome-LOX-1 antibody highly and specifically bound to the LOX-1 antigen, whereas, very little liposome-nIgG bound. Notably, LOX-1 probes cleared slowly compared to nIgG probes in the Apo $E^{-/-}$ mice initially. The slower clearance might be related to cycling of binding of the LOX-1 probe to LOX-1 antigen in the atherosclerotic plaque as well as to soluble LOX-1 fragments in the plasma; however, both probes were equally and rapidly cleared in the C57BL/6 mice. The slow clearance of LOX-1 probe in the Apo $E^{-/-}$ mice may allow greater binding of LOX-1 antibody to LOX-1 antigen and enhance its uptake within the plaque. The half life of ^{111}In is 2.8 days. The majority of LOX-1 probe cleared from the blood pool 24 hours after injection, providing the rationale for imaging at 24 hrs after injection. As expected with liposomes, a significant amount of the probe accumulated in the liver and spleen, however this did not affect image quality since we scanned from the aortic root to arch.

LOX-1 imaging signal and vulnerability of atherosclerotic plaque to rupture

Over the last decade, it has become evident that rupture-prone atherosclerotic plaques are seen in a majority of patients with life-threatening coronary syndromes. It is widely appreciated that the shoulder region of plaque is a common site in plaque rupture because it has more inflammation, apoptosis, shear stress and gene expression (34–36).

We found that the LOX-1 probe was localized primarily in the shoulder region of plaques in the atherosclerotic $LDLR^{-/-}$ mice. This finding correlated with the distribution of LOX-1 expression seen by immunostaining. Importantly, we found that the LOX-1 probe co-localized with macrophages, apoptotic cells and MMP9 expressing cells. A recent study in atherosclerotic rabbits (33) found that ^{99m}Tc-LOX-1 antibody accumulated selectively in atheromatous lesions with large numbers of macrophages and extracellular lipid deposits but fewer smooth muscle cells and collagen fibers. Our results are important since we showed co-

localization of the LOX-1 probe to rupture-prone atherosclerotic regions in murine models that are often used for developing molecular targeted diagnostic and therapeutic approaches.

Molecular imaging targeted to LOX-1 for detecting atherosclerotic plaque

No single imaging modality can provide overall structural, functional, and molecular information as each modality has its own strengths and weaknesses. Nuclear imaging has high sensitivity, but low spatial resolution. MRI has high spatial resolution, providing clear information on anatomy and function, but the sensitivity is not as high as with nuclear. Multimodality molecular imaging techniques can provide complementary information to define the characteristics of atherosclerotic plaque (37,38). In the current study, we found that SPECT/CT clearly showed hotspots in the atherosclerotic region of aortic arch in Apo $E^{-/-}$ mice injected with the LOX-1, but not the nIgG probe. Likewise, MRI demonstrated strong post-Gd enhancement in atherosclerotic plaques from the aortic root to the arch in the $LDLR^{-/-}$ mice injected with LOX-1 probe with no post-Gd enhancement in the same mice injected with nIgG probe. The specificity of LOX-1 imaging signal was further delineated using LDLR $^{-/-}$ mice with LOX-1 abrogation that showed a marked reduction in LOX-1 probe binding and post-Gd enhancement. Previous studies have shown a marked reduction in atherogenesis in these double knockout mice (11).

These data from two different mouse models and two different imaging modalities adequately validate that LOX-1 can be used as a target for molecular imaging to detect atherosclerotic plaques. Other imaging studies (13,17,21,30) have focused on the abdominal aorta. A weakness of those studies relates to the accumulation of probes in the liver, spleen and kidney which are adjacent to the abdominal aorta. To overcome this limitation, we focused on the aortic root and arch. these regions have more extensive atherosclerosis than the abdominal aorta in the mice, but more importantly one can avoid false positive data from probe accumulation in the liver and spleen.

In summary, we show that LOX-1 can be used as a molecular imaging target with high binding affinity, sensitivity, and selectivity in atherosclerotic plaques. LOX-1 targeting provides important information pertaining to the vulnerability of atherosclerotic plaques. These multimodality molecular imaging techniques may evolve into clinically relevant non-invasive tools for detecting and monitoring rupture-prone plaques. These techniques may also be used to assess the efficacy of novel treatments that induce plaque regression and stabilization.

The authors acknowledge R. Jack Roy and Joseph Pole for assistance with the MRI and SPECT/CT, respectively, Joseph DiMaria for assistance with animals, and Christopher T. Sica, Weitian Chen and Hao Tan for assistance with image reconstruction. The authors also acknowledge helpful discussion with Brett Blackman and Kimberly Kelly. This work was supported by the University of Virginia-Coulter Foundation Translational Research Partnership, the Nuclear Cardiology Foundation and NIH T32 HL007355.

1. Witztum JL, Steinberg D. Role of oxidized low density lipoprotein in atherogenesis. *J Clin Invest.* 1991;88:1785–1792. [PMC free article] [PubMed]

2. Mehta JL, Chen J, Hermonat PL, Romeo F, Novelli G. Lectin-like, oxidized low-density lipoprotein receptor-1 (LOX-1): a critical player in the development of atherosclerosis and related disorders. *Cardiovasc Res.* 2006;69:36–45. [PubMed]

3. Sawamura T, Kume N, Aoyama T, et al. An endothelial receptor for oxidized low-density lipoprotein. *Nature.* 1997;386:73–77. [PubMed]

4. Cominacini L, Pasini AF, Garbin U, et al. Oxidized low density lipoprotein (ox-LDL) binding to ox-LDL receptor-1 in endothelial cells induces the activation of NF-κB through an increased production of intracellular reactive oxygen species. *J Biol Chem.* 2000;275:12633–12638. [PubMed]

5. Li D, Mehta JL. Upregulation of endothelial receptor for oxidized LDL (LOX-1) by oxidized LDL and implications in apoptosis of human coronary artery endothelial cells: evidence from use of antisense LOX-1 mRNA and chemical inhibitors. *Arterioscler Thromb Vasc Biol.* 2000;20:1116–1122. [PubMed]

6. Terasaka N, Wang N, Yvan-Charvet L, Tall AR. High-density lipoprotein protects macrophages from oxidized low-density lipoprotein-induced apoptosis by promoting efflux of 7-ketocholesterol via ABCG1. *Proc Natl Acad Sci U S A.* 2007;104:15093–15098. [PMC free article] [PubMed]

7. Li D, Mehta JL. Antisense to LOX-1 inhibits oxidized LDL-mediated upregulation of monocyte chemoattractant protein-1 and monocyte adhesion to human coronary artery endothelial cells. *Circulation.* 2000;101:2889–2895. [PubMed]

8. Yoshida H, Kondratenko N, Green S, Steinberg D, Quehenberger O. Identification of the lectin-like receptor for oxidized low-density lipoprotein in human macrophages and its potential role as a scavenger receptor. *Biochem J.* 1998;334:9–13. [PMC free article] [PubMed]

9. Li D, Liu L, Chen H, Sawamura T, Mehta JL. LOX-1, an oxidized LDL endothelial receptor, induces CD40/CD40L signaling in human coronary artery endothelial cells. *Arterioscler Thromb Vasc Biol.* 2003;23:816–821. [PubMed]

10. Li D, Liu L, Chen H, Sawamura T, Mehta JL. LOX-1 Mediates Oxidized LDL-Induced the Expression and Activation of Matrix Metalloproteinases (MMPs) in Human Coronary Artery Endothelial Cells. *Circulation.* 2003;107:612–617. [PubMed]

11. Mehta JL, Sanada N, Hu CP, Chen J, Dandapat A, Sugawara F, Takeya M, Inoue K, Kawase Y, Jishage K, Suzuki H, Satoh H, Schnackenberg L, Beger R, Hermonat PL, Thomas M, Sawamura T. Deletion of LOX-1 reduces atherogenesis in LDLR knockout mice fed high cholesterol diet. *Circulation Research.* 2007;100:1634–1642. [PubMed]

12. Li D, Chen H, Staples ED, Ozaki K, Annex B, Singh BK, Vermani R, Mehta JL. Oxidized low-density lipoprotein receptor LOX-1 and apoptosis in human atherosclerotic lesions. *J Cardiovasc Pharmacol Ther.* 2002;7:147–153. [PubMed]

13. Amirbekian V, Lipinski MJ, Briley-Saebo KC, Amirbekian S, Aguinaldo JG, Weinreb DB, Vucic E, Frias JC, Hyafil F, Mani V, Fisher EA, Fayad ZA. Detecting and assessing macrophages in vivo to evaluate atherosclerosis noninvasively using molecular MRI. *Proc Natl Acad Sci U S A.* 2007;104:961–966. [PMC free article] [PubMed]

14. Hayashida K, Kume N, Murase T, Minami M, Nakagawa D, Inada T, Tanaka M, Ueda A, Kominami G, Kambara H, Kimura T, Kita T. Serum soluble lectin-like oxidized low-density lipoprotein receptor-1 levels are elevated in acute coronary syndrome: a novel marker for early diagnosis. *Circulation.* 2005;112:812–818. [PubMed]

15. Kolodgie FD, Narula J, Haider N, Virmani R. Apoptosis in atherosclerosis. Does it contribute to plaque instability? *Cardiol Clin.* 2001;19:127–139. [PubMed]

16. Littlewood TD, Bennett MR. Apoptotic cell death in atherosclerosis. *Curr Opin Lipidol.* 2003;14:469–475. [PubMed]

17. Johnson JL, Baker AH, Oka K, Chan L, Newby AC, Jackson CL, George SJ. Suppression of atherosclerotic plaque progression and instability by tissue inhibitor of metalloproteinase-2: involvement of macrophage migration and apoptosis. *Circulation.* 2006;113:2435–2444. [PubMed]

18. Sarai M, Hartung D, Petrov A, Zhou J, Narula N, Hofstra L, Kolodgie F, Isobe S, Fujimoto S, Vanderheyden JL, Virmani R, Reutelingsperger C, Wong ND, Gupta S, Narula J. Broad and specific caspase inhibitor-induced acute repression of apoptosis in atherosclerotic lesions evaluated by radiolabeled annexin A5 imaging. *J Am Coll Cardiol.* 2007;50:2305–2312. [PubMed]

19. Halvorsen B, Otterdal K, Dahl TB, Skjelland M, Gullestad L, Øie E, Aukrust P. Atherosclerotic plaque stability--what determines the fate of a plaque? *Prog Cardiovasc Dis.* 2008;51:183–194. [PubMed]

20. Newby AC. Metalloproteinase expression in monocytes and macrophages and its relationship to atherosclerotic plaque instability. *Arterioscler Thromb Vasc Biol.* 2008;28:2108–2114. [PubMed]

21. Hyafil F, Cornily JC, Feig JE, Gordon R, Vucic E, Amirbekian V, Fisher EA, Fuster V, Feldman LJ, Fayad ZA. Noninvasive detection of macrophages using a nanoparticulate contrast agent for computed tomography. *Nat Med.* 2007;13:636–641. [PubMed]

22. Shah PK, Falk E, Badimon JJ, Fernandez-Ortiz A, Mailhac A, Villareal-Levy G, Fallon JT, Regnstrom J, Fuster V. Human monocyte-derived macrophages induce collagen breakdown in fibrous caps of atherosclerotic plaques. Potential role of matrix-degrading metalloproteinases and implications for plaque rupture. *Circulation.* 1995;92:1565–1569. [PubMed]

23. Ohshima S, Petrov A, Fujimoto S, Zhou J, Azure M, Edwards DS, Murohara T, Narula N, Tsimikas S, Narula J. Molecular imaging of matrix metalloproteinase expression in atherosclerotic plaques of mice deficient in apolipoprotein e or low-density-lipoprotein receptor. *J Nucl Med.* 2009;50:612–617. [PubMed]

24. Deguchi JO, Aikawa M, Tung CH, Aikawa E, Kim DE, Ntziachristos V, Weissleder R, Libby P. Inflammation in atherosclerosis: visualizing matrix metalloproteinase action in macrophages in vivo. *Circulation.* 2006;114:55–62. [PubMed]

25. Briley-Saebo KC, Shaw PX, Mulder WJ, Choi SH, Vucic E, Aguinaldo JG, Witztum JL, Fuster V, Tsimikas S, Fayad ZA. Targeted molecular probes for imaging atherosclerotic lesions with magnetic resonance using antibodies that recognize oxidation-specific epitopes. *Circulation.* 2008;117:3206–3215. [PubMed]

26. Nahrendorf M, Jaffer FA, Kelly KA, Sosnovik DE, Aikawa E, Libby P, Weissleder R. Noninvasive vascular cell adhesion molecule-1 imaging identifies inflammatory activation of cells in atherosclerosis. *Circulation.* 2006;114:1504–1511. [PubMed]

27. Botnar RM, Perez AS, Witte S, Wiethoff AJ, Laredo J, Hamilton J, Quist W, Parsons EC, Jr, Vaidya A, Kolodziej A, Barrett JA, Graham PB, Weisskoff RM, Manning WJ, Johnstone MT. In vivo molecular imaging of acute and subacute thrombosis using a fibrin-binding magnetic resonance imaging contrast agent. *Circulation.* 2004;109:2023–2029. [PMC free article] [PubMed]

28. Winter PM, Neubauer AM, Caruthers SD, Harris TD, Robertson JD, Williams TA, Schmieder AH, Hu G, Allen JS, Lacy EK, Zhang H, Wickline SA, Lanza GM. Endothelial alpha(v)beta3 integrin-targeted fumagillin nanoparticles inhibit angiogenesis in atherosclerosis. *Arterioscler Thromb Vasc Biol.* 2006;26:2103–2109. [PubMed]

29. Winter PM, Caruthers SD, Zhang H, Williams TA, Wickline SA, Lanza GM. Antiangiogenic synergism of integrin-targeted fumagillin nanoparticles and atorvastatin in atherosclerosis. *JACC Cardiovasc Imaging.* 2008;1:624–634. [PMC free article] [PubMed]

30. Kakutani M, Masaki T, Sawamura T. A platelet-endothelium interaction mediated by lectin-like oxidized low-density lipoprotein receptor-1. *Proc Natl Acad Sci U S A.* 2000;97:360–364. [PMC free article] [PubMed]

31. Delneste Y, Magistrelli G, Gauchat J, Haeuw J, Aubry J, Nakamura K, Kawakami-Honda N, Goetsch L, Sawamura T, Bonnefoy J, Jeannin P. Involvement of LOX-1 in dendritic cell-mediated antigen cross-presentation. *Immunit* . 2002;17:353–362. [PubMed]

32. Kuge Y, Kume N, Ishino S, Takai N, Ogawa Y, Mukai T, Minami M, Shiomi M, Saji H. Prominent lectin-like oxidized low density lipoprotein (LDL) receptor-1 (LOX-1) expression in atherosclerotic lesions is associated with tissue factor expression and apoptosis in hypercholesterolemic rabbits. *Biol Pharm Bull.* 2008;31:1475–1482. [PubMed]

33. Ishino S, Mukai T, Kuge Y, Kume N, Ogawa M, Takai N, Kamihashi J, Shiomi M, Minami M, Kita T, Saji H. Targeting of lectinlike oxidized low-density lipoprotein receptor 1 (LOX-1) with 99mTc-labeled anti-LOX-1 antibody: potential agent for imaging of vulnerable plaque. *J Nucl Med.* 2008;49:1677–1685. [PubMed]

34. Kumar RK, Balakrishnan KR. Influence of lumen shape and vessel geometry on plaque stresses: possible role in the increased vulnerability of a remodelled vessel and the "shoulder" of a plaque. *eart.* 2005;91:1459–1465. [PMC free article] [PubMed]

35. Björkerud S, Björkerud B. Apoptosis is abundant in human atherosclerotic lesions, especially in inflammatory cells (macrophages and T cells), and may contribute to the accumulation of gruel and plaque instability. *Am J Pathol.* 1996;149:367–380. [PMC free article] [PubMed]

36. Pasterkamp G, Schoneveld AH, van der Wal AC, Hijnen DJ, van Wolveren WJ, Plomp S, Teepen HL, Borst C. Inflammation of the atherosclerotic cap and shoulder of the plaque is a common and locally observed feature in unruptured plaques of femoral and coronary arteries. *Arterioscler Thromb Vasc Biol.* 1999;19:54–58. [PubMed]

37. Lee S, Chen X. Dual-modality probes for in vivo molecular imaging. *Molecular Imaging.* 2009;8:87–100. [PubMed]

38. Nahrendorf M, Zhang H, Hembrador S, Panizzi P, Sosnovik DE, Aikawa E, Libby P, Swirski FK, Weissleder R. Nanoparticle PET-CT imaging of macrophages in inflammatory atherosclerosis. *Circulation.* 2008;117:379–387. [PMC free article] [PubMed]

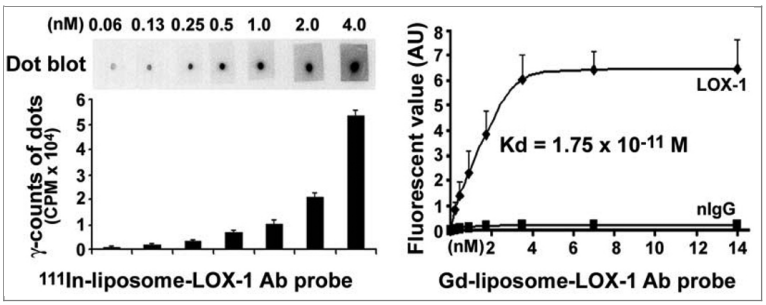
(nM) 0.06 0.13 0.25 0.5 1.0 2.0 4.0
Dot blot
γ-counts of dots (CPM x 10⁴)
¹¹¹In-liposome-LOX-1 Ab probe
Fluorescent value (AU)
LOX-1
Kd = 1.75 x 10⁻¹¹ M
nIgG
(nM)
Gd-liposome-LOX-1 Ab probe

Figure 1

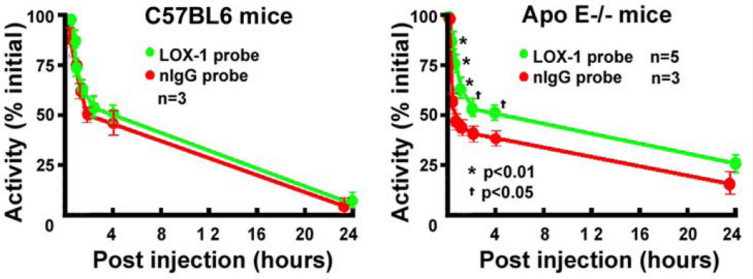

Bio-distribution of LOX-1 probe in Apo E-/- mice (%24 hr blood activity)

Lung	Heart	Kidney	Spleen	Muscle	Liver	Fat	Gut	Urine
52±15	19±4	37±12	933±108	8±4	837±284	4±3	7±2	9±4

Figure 2

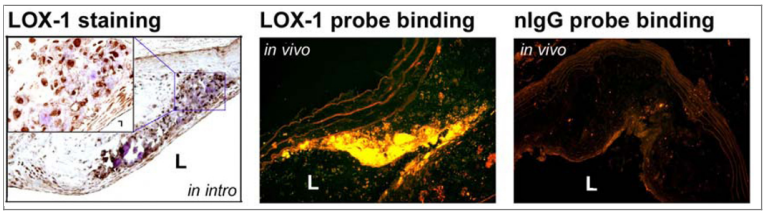
LOX-1 staining
LOX-1 probe binding
nIgG probe binding
in vivo
in vivo
L
L
L
in intro

Figure 3

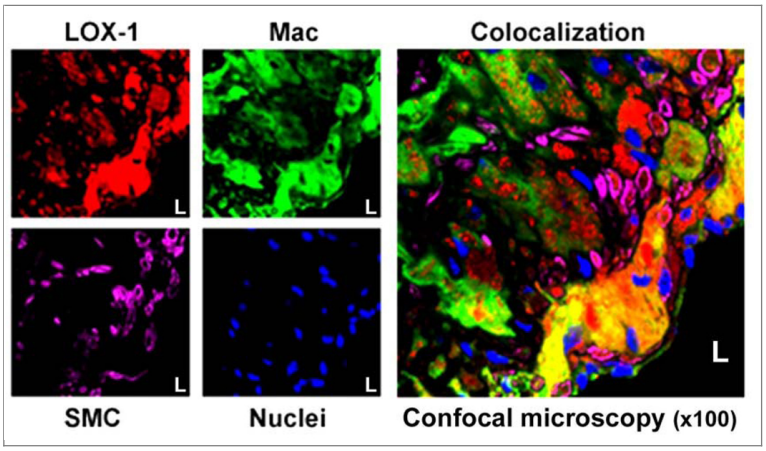
LOX-1
Mac
Colocalization
L
L
L
L
L
SMC
Nuclei
Confocal microscopy (x100)

Figure 4

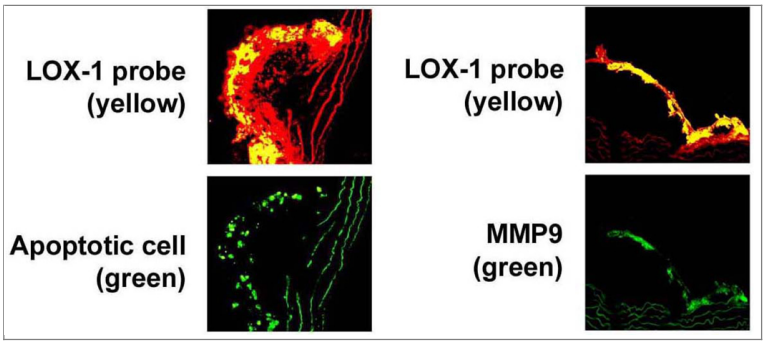
LOX-1 probe
(yellow)
LOX-1 probe
(yellow)
Apoptotic cell
(green)
MMP9
(green)

Figure

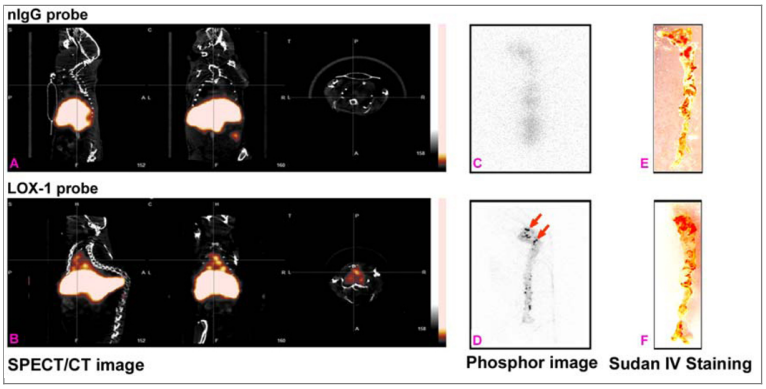
nIgG probe
A
C
E
LOX-1 probe
B
D
F
SPECT/CT image
Phosphor image
Sudan IV Staining

Figure

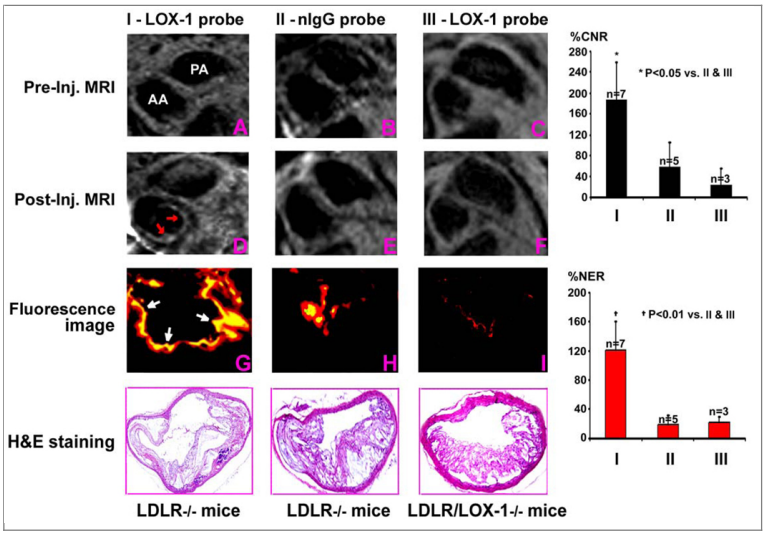
I - LOX-1 probe
II - nIgG probe
III - LOX-1 probe
Pre-Inj. MRI
Post-Inj. MRI
Fluorescence image
H&E staining
PA
AA
A
B
C
D
E
F
G
H
I
%CNR
* P<0.05 vs. II & III
n=7
n=5
n=3
%NER
* P<0.01 vs. II & III
LDLR-/- mice
LDLR-/- mice
LDLR/LOX-1-/- mice

Figure 7

This document was created with Win2PDF available at http://www.win2pdf.com.
The unregistered version of Win2PDF is for evaluation or non-commercial use only.
This page will not be added after purchasing Win2PDF.